4.2 Phase Shifts of p-^{3}He Scattering

Abstract. A method employing sinle-energy phase-shift analysis of p-^{3}He scattering is developed by using the S-matrix in the Matsuda-Watari representation. This method can be applied for analyses in the low-energy region and also in the inelastic region. Phase-shift solutions of p-^{3}He scattering are given at $T_L = 4.0$, 5.5, 6.8, 8.5, 9.5 and 19.48 MeV. (Prog. Theor. Phys. **103** (2000), 107.)

4.2.1 Introduction

Since the 1950s, experiments on p-^{3}He scattering and their phase-shift analyses (PSA) have been performed with great interest in nuclei of mass number 4. Recently, an experiment on the ^{3}He$(d,p)^4$He reaction with incident deuterons of kinetic energy 270 MeV was carried out at RIKEN[114]. Oryu et al.[115] attempted theoretical analyses of these experimental data by using the multi-channel Faddeev-equations, where the system of p-n-^{3}He plays an important role. The nucleon-^{3}He potentials are needed to solve these equations. In their phenomenological approach, Oryu et al. evaluated the p-^{3}He and n-^{3}He potentials by modifying the Paris nucleon-nucleon potential with the Ernst-Shakin-Thaler approximation so as to fit the low energy p-^{3}He and n-^{3}He phase shifts. In this approach, model-independent solutions of the phase shifts of p-^{3}He and n-^{3}He scattering are required in a wide range of incident-nucleon energies.

The PSA of p-^{3}He scattering has been carried out by Lowen[120], Frank and Gammel[121], Tombrello et al.[122] and Clegg et al.[123], making use of only the experimental data on $d\sigma/d\Omega$. Tombrello[112] obtained the phase shifts in the states of orbital angular momentum $\ell \leq 2$ with the PSA of $d\sigma/d\Omega$ and proton polarization data with incident proton energies in the laboratory system of $T_L = 1.0 - 11.5$ MeV, where the relation of D-wave phase shifts $\delta(^3D_1) = \delta(^3D_2) = \delta(^3D_3)$ was assumed. Improved PSA were carried out by Morrow and Haeberli[124], McSherry and Baker[125] and Szaloky and Seiler[126]. Beltramin, Frate and Pisent[127] determined the phase shifts of $\ell \leq 2$ with PSA using the data on $d\sigma/d\Omega$, proton polarization, ^{3}He polarization and Wolfenstein parameters in the energy region $T_L \leq 10.0$ MeV. Recently, Alley and Knutson[113] carried out both energy-dependent and single-energy PSA on eight kinds of data in the energy region $T_L \lesssim 12.0$ MeV and determined the phase shifts of $\ell \leq 3$, with the approximations $\delta(^3D_1) = \delta(^3D_2) = \delta(^3D_3)$ and $\delta(^1F_3) = \delta(^3F_2) = \delta(^3F_3) = \delta(^3F_4)$. The first inelastic channel, p+^{3}He $\to d + 2p$, opens at $T_L = 7.3$ MeV, and the second one, p+^{3}He $\to n + 3p$, opens at $T_L = 10.3$ MeV. The cross sections of these reactions are very small below 10 MeV,[112] and some groups have carried out the PSA by neglecting these inelastic effects. For $T_L = 19 - 48$ MeV, Murdoch et al.[128] evaluated the inelastic effect and extracted rough values for the phase shifts.

Recently, experimental data on various kinds of spin-correlation coefficients of p-^{3}He scattering have been accumulated for $T_L \lesssim 20$ MeV. These data give us incentive to carry out the single-energy PSA in this energy region more completely. Moreover, in the intermediate energy region $T_L = 20 - 300$ MeV, the spin-correlation parameters have also been accumulated at some energy points at which the single-energy PSA should be carried out.

The parametrization of the S matrix given by Blatt and Biedenharn[129] (BB) has been used in the usual PSA of p-^{3}He scattering, because the inelastic effects do not have to be taken into account for energies of $T_L \lesssim 10$ MeV. We have developed the PSA of p-^{3}He scattering by using the S matrix in the Matsuda-Watari (MW) representation[29] in order to evaluate the inelastic effect, which can be applied for analyses in the low energy region and also in the intermediate region. In the elastic region, the MW phase shifts are equivalent to the nuclear-bar phase shifts introduced by Stapp, Ypsilantis and Metropolis[37]. Here we perform the single-energy PSA of p-^{3}He scattering at $T_L = 4.0$, 5.5, 6.8, 8.5, 9.5 and 19.48 MeV, and give the result.

In the next subsection, we briefly give the formulation of the PSA of p-^{3}He scattering. In subsection 4.2.3 we give the experimental data used in the present analyses. In subsection 4.2.4 the solutions we obtain are given and compared with that of Alley and Knutson. Subsection 4.2.5 is devoted to concluding remarks.

4.2.2 Method of phase-shift analysis

Scattering matrix

Let $\chi^{(n)}$ be a vector with four components which represents the state of initial spin n. The scattering state wave function may be written as a vector:

$$\Psi^{(n)} = e^{i(\boldsymbol{k}_i\cdot\boldsymbol{r})}\chi^{(n)} + f^{(n)}\frac{e^{ikr}}{r},$$

$$f^{(n)} = M\chi^{(n)}. \tag{4.29}$$

Here k is the wave number of the proton in the c.m.s., and M is a 4×4 matrix operating on the initial spin state.

The general form of M matrix can be decomposed into six invariant amplitudes as

$$M = \frac{1}{2}[a + b + (a-b)(\boldsymbol{\sigma}_1\cdot\boldsymbol{n})(\boldsymbol{\sigma}_2\cdot\boldsymbol{n}) + (c+d)(\boldsymbol{\sigma}_1\cdot\boldsymbol{m})(\boldsymbol{\sigma}_2\cdot\boldsymbol{m})$$

$$+(c-d)(\boldsymbol{\sigma}_1\cdot\boldsymbol{l})(\boldsymbol{\sigma}_2\cdot\boldsymbol{l}) + e(\boldsymbol{\sigma}_1+\boldsymbol{\sigma}_2)\cdot\boldsymbol{n} + f(\boldsymbol{\sigma}_1-\boldsymbol{\sigma}_2)\cdot\boldsymbol{n}], \tag{4.30}$$

subject to its invariance under space rotations, reflections and time reversal[130, 118]. The Pauli matrices $\boldsymbol{\sigma}_1$ and $\boldsymbol{\sigma}_2$ act on the spin wave functions of the proton and ^{3}He, respectively, and the characters $\boldsymbol{l}, \boldsymbol{m}$ and $\boldsymbol{n}$ are the unit vectors defined by

$$\boldsymbol{l} = \frac{\boldsymbol{p}_f + \boldsymbol{p}_i}{|\boldsymbol{p}_f + \boldsymbol{p}_i|}, \qquad \boldsymbol{m} = \frac{\boldsymbol{p}_f - \boldsymbol{p}_i}{|\boldsymbol{p}_f - \boldsymbol{p}_i|}, \qquad \boldsymbol{n} = \frac{\boldsymbol{p}_i \times \boldsymbol{p}_f}{|\boldsymbol{p}_i \times \boldsymbol{p}_f|}, \tag{4.31}$$

where $\boldsymbol{p}_i$ and $\boldsymbol{p}_f$ are the momenta in the c.m.s. in the initial and final states, respectively.

The partial wave expansion of M matrices for p-^{3}He scattering is given by

$$M_{ss_zs's'_z} = C(\theta)\delta_{s,s'}\delta_{s_z,s'_z} + 4\pi\sum_{\ell,\ell',J}\sqrt{\frac{2\ell'+1}{4\pi}}Y_\ell^{s'_z-s_z}(\theta,\phi)$$

$$\times C_{\ell s}(J, s'_z, s'_z - s_z, s_z)C_{\ell' s'}(J, s'_z, 0, s_z)h^J_{\ell s,\ell' s'}. \tag{4.32}$$

Here s and s' are the total spins of the p-^{3}He system in the final and initial states, respectively, and s_z and $s_{z'}$ are their z-components. (θ, ϕ) is the scattering angle in the c.m.s. $C_{\ell s}$ are the

Clebsch-Gordan coefficients, and $Y_\ell^m(\theta,\phi)$ are the normalized spherical harmonics. $C(\theta)$ is the Coulomb amplitude. Finally, $h^J_{\ell s,\ell' s'}$ are the partial wave amplitudes of p-^{3}He scattering, which have the following relation to the S matrix:

$$h^J_{\ell s,\ell' s'} = \frac{1}{2ik}(S^J_{\ell s,\ell' s'} - \delta_{\ell,\ell'}\delta_{s,s'})e^{i(\Phi_\ell+\Phi_{\ell'})}. \tag{4.33}$$

Here Φ_ℓ is the Coulomb phase shift and k is the wave number in the c.m.s., ℓ and ℓ' are the orbital angular momenta in the final and initial states, respectively, and J is the total angular momentum.

Parametrization of the scattering matrix

In the PSA of p-^{3}He scattering, only the BB parametrization has been used to this time. Recently, Mefford and Landau[131] gave an expression of the S matrix followed by the parametrization of Stapp, Ypsilantis and Metropolis[37]. Here we adopt the S matrix in the MW parametrization in order to develop the high-energy PSA program. In this representation, the S matrices are as follows:
For singlet state,

$$S_\ell = \eta_\ell e^{2i\delta_\ell}, \tag{4.34}$$

for uncoupled waves in the triplet state,

$$S_{\ell,J} = \eta_{\ell,J} e^{2i\delta_{\ell,J}}, \tag{4.35}$$

and for coupled waves between $\ell = J-1$ and $\ell = J+1$ in the triplet state,

$$S_J = \begin{pmatrix} \sqrt{1-|\rho_J|^2}\ \eta_+ e^{2i\delta_+} & i\rho_J\sqrt{\eta_+\eta_-}e^{i(\delta_++\delta_-)} \\ i\rho_J\sqrt{\eta_+\eta_-}e^{i(\delta_++\delta_-)} & \sqrt{1-|\rho_J|^2}\ \eta_- e^{2i\delta_-} \end{pmatrix}. \tag{4.36}$$

In this equation, the $\delta_\pm$, ρ_J and $\eta_\pm$ are the phase shifts, the mixing parameters and the reflection parameters, respectively. For couple waves of $\ell = J$ between singlet and triplet states,

$$S_J^{ST} = \begin{pmatrix} \sqrt{1-|\rho_J^{(S)}|^2}\ \eta_J e^{2i\delta_J} & i\rho_J^{(S)}\sqrt{\eta_J\eta_{J,J}}e^{i(\delta_J+\delta_{J,J})} \\ i\rho_J^{(S)}\sqrt{\eta_J\eta_{J,J}}e^{i(\delta_J+\delta_{J,J})} & \sqrt{1-|\rho_J^{(S)}|^2}\ \eta_{J,J} e^{2i\delta_{J,J}} \end{pmatrix}. \tag{4.37}$$

In the elastic region, this representation is equivalent to that given by Stapp, Ypsilantis and Metropolis[37], since $\eta_{\ell,J} = 1$.

4.2.3 Experimental data on p-^{3}He scattering at low energies

We have compiled a database of the experimental data on p-^{3}He scattering with $T_L \leq$ 20 MeV, which were obtained from 1956 to 1993, and use it to investigate the energy points where a relatively large amount of data have been accumulated. We performed the single-energy PSA of p-^{3}He scattering at T_L = 4.0, 5.5, 6.8, 8.5, 9.5 and 19.48 MeV, with the energy bin $\Delta T_L = \pm$ 0.5 MeV, where the data on $d\sigma/d\Omega$, the proton analyzing power, the ^{3}He analyzing power and other spin-correlation coefficients are accumulated. The results are given in Table 4.1. The experimental quantities are defined as follows.

Differential cross section :

$$d\sigma/d\Omega = (0,0;0,0). \tag{4.38}$$

Analyzing powers (Polarizations) :

$$\begin{aligned} A_{y0} &= (N,0;0,0) = (0,0;N,0), \\ A_{0y} &= (0,N;0,0) = (0,0;0,N). \end{aligned} \tag{4.39}$$

Spin-correlation coefficients :

$$\begin{aligned} A_{xx} &= (S,S;0,0), \\ A_{xz} &= (S,L;0,0), \\ A_{yy} &= (N,N;0,0), \\ A_{zx} &= (L,S;0,0), \\ A_{zz} &= (S,S;0,0). \end{aligned} \tag{4.40}$$

Wolfenstein parameters :

$$\begin{aligned} R &= (S,0;S,0), \\ A &= (L,0;S,0), \\ D &= (N,0;N,0). \end{aligned} \tag{4.41}$$

Here the bracket symbols $(i,j;i',j')$ denote the spin directions of the proton beam, the ^{3}He target, the scattered proton and the recoil ^{3}He, respectively. Also, L indicates the direction of motion, N the normal to the scattering plane and S the directions of $N \times L$. Here, an entry of 0 implies the non-observation of a spin state.

The data on $d\sigma/d\Omega$ obtained by McDonald, Haeberli and Morrow[132] are important in our PSA at 4.0 and 6.8 MeV. Clegg et al.[123] obtained experimental data on the excitation function at angles in the c.m.s. $\theta_{\rm cm}$ of 90.0°, 125.3° and 161.2° from 4.4 to 10.4 MeV in steps of 0.2 MeV and measured the angular distributions of $d\sigma/d\Omega$ for $T_L = 4.55 - 11.48$ MeV. Alley and Knutson[134] measured A_{y0}, A_{0y} and the other spin-correlation coefficients at selected energy points. These data also play an important role for our PSA.

Sourkes et al.[140] reported the results of their experiments for the total reaction cross section σ_r in the range $T_L = 18 - 48$ MeV. We include their datum at $T_L = 19.55$ MeV in our database in order to evaluate the inelastic effect.

In Table 4.1, the experimental data of the groups corresponding to the references with the asterisks ($*$) are not used in the present analyses. The energy dependence of the A_{y0} data at 3.54 MeV in Ref. [133] and the $d\sigma/d\Omega$ data at 6.5 MeV and 8.34 MeV in Ref. [136] are remarkably inconsistent with those of the other groups. We observe the strong energy dependence of $d\sigma/d\Omega$ around 6.8 MeV and do not use the 21 data points for $d\sigma/d\Omega$ at 6.52 MeV in Ref. [123]. Accordingly, the 16 data points for $d\sigma/d\Omega$ at 6.82 MeV in Ref. [132] have a principal role in the data-fitting at 6.8 MeV. The A_{0y} datum at $\theta_{\rm cm} = 127.4°$, $T_L =$ 5.9 MeV in Ref. [125] is not used in the present analysis, because its value is quite different from the ones by the other groups and give the bad influence to the solution.

Table 4.1: The list of experimental data used in the present analyses at T_L = 4.0, 5.5, 6.8, 8.5, 9.5 and 19.48 MeV. $\theta_{\rm cm}$ is the scattering angle of the proton in the c.m.s. in degrees, and n_j is the renormalization parameter. The correspondence of the data references in the table to the reference numbers given in the bibliography are as follows : MC(64)[132], CL(64)[123], DR(66)[133], MO(69)[124], AL(93)[134], MC(69)[135], BR(60)[136], WE(78)[137], LO(56)[111], HU(71)[138], BA(71)[139], SO(76)[140]. The data of the groups corresponding to the references with the asterisks (*) are not used.

T_L (MeV)	Observables	Measured energy	$\theta_{\rm cm}$ (degree)	n_j	No. of data	Ref.
4.0	$d\sigma/d\Omega$	4.00	18.6 ~ 170.6	1.0	16	MC(64)
		4.40	90.0 ~ 161.2	1.0942	3	CL(64)
	A_{y0}	3.54	67.8 ~ 134.7		14	DR(66)*
		3.84	67.8 ~ 138.8	0.9428	15	DR(66)
		4.15	67.8 ~ 142.8	1.0	16	DR(66)
		4.46	67.8 ~ 134.7	0.9287	14	DR(66)
		4.00	27.1 ~ 123.8	1.0	11	MO(69)
		4.01	26.6 ~ 159.7	1.0	27	AL(93)
		4.01	49.3 ~ 126.1	1.0	8	AL(93)
		4.05	60.1 ~ 109.9	1.0	4	MC(64)
	A_{0y}	3.86	58.0 ~ 127.4	1.0	4	MC(70)
		4.01	49.3 ~ 126.1	1.0	8	AL(93)
		4.38	58.0 ~ 110.0	1.0	2	MC(70)
	A_{yy}	4.01	49.3 ~ 126.1	1.0	8	AL(93)
5.5	$d\sigma/d\Omega$	5.19	90.0 ~ 161.2	1.0	3	CL(64)
		5.38	90.0 ~ 161.2	1.0	3	CL(64)
		5.51	18.6 ~ 170.6	1.0	16	MC(64)
		5.51	27.6 ~ 166.6	1.0	22	CL(64)
		5.62	90.0 ~ 161.2	1.0531	3	CL(64)
		5.79	90.0 ~ 161.2	1.0662	3	CL(64)
		5.99	90.0 ~ 161.2	1.0977	3	CL(64)
	A_{y0}	5.51	24.5 ~ 155.8	1.0	14	MO(69)
		5.52	59.1 ~ 109.9	1.0	4	MC(64)
		5.54	26.6 ~ 159.7	1.0	27	AL(93)
		5.54	49.3 ~ 150.6	1.0	10	AL(93)
	A_{0y}	5.90	58.0 ~ 110.0	1.0	3	MC(70)
		5.54	49.3 ~ 150.6	1.0	10	AL(93)
	A_{xx}	5.54	49.3 ~ 142.9	1.0	5	AL(93)
	A_{xz}	5.54	49.3 ~ 142.9	1.0	5	AL(93)
	A_{yy}	5.54	49.3 ~ 150.6	1.0	10	AL(93)
	A_{zz}	5.54	49.3 ~ 142.9	1.0	5	AL(93)
6.8	$d\sigma/d\Omega$	6.39	90.0 ~ 161.2	0.9303	3	CL(64)
		6.50	13.3 ~ 160.0		35	BR(60)*
		6.52	27.6 ~ 166.6		21	CL(64)*
		6.59	90.0 ~ 161.2	0.9669	3	CL(64)
		6.60	90.0 ~ 161.2	0.9706	3	CL(64)
		6.79	90.0 ~ 161.2	1.0	3	CL(64)
		6.82	18.6 ~ 170.6	1.0	16	MC(64)
		6.99	90.0 ~ 161.2	1.0	3	CL(64)
		7.18	90.0 ~ 161.2	1.0	3	CL(64)

(continued)

Table 4.1: (continued)

T_L (MeV)	Observables	Measured energy	$\theta_{\rm cm}$ (degree)	n_j	No. of data	Ref.
	A_{y0}	6.82	24.5 ~ 155.8	1.0	14	MO(69)
		6.83	59.1 ~ 132.7	1.0	5	MC(64)
		7.03	26.6 ~ 159.7	1.0	27	AL(93)
		7.03	49.3 ~ 150.6	1.0	10	AL(93)
	A_{0y}	6.91	58.0 ~ 127.4	1.0	4	MC(70)
		7.03	49.3 ~ 150.6	1.0	10	AL(93)
	A_{yy}	7.03	49.3 ~ 150.6	1.0	10	AL(93)
	R	6.82	43.6 ~ 58.9	1.3288	2	WE(78)
	A	6.82	43.6 ~ 58.9	0.7620	2	WE(78)
	D	6.82	43.6 ~ 58.9	1.0	2	WE(78)
8.5	$d\sigma/d\Omega$	8.19	90.0 ~ 161.2	0.9560	3	CL(64)
		8.30	13.3 ~ 160.0		38	BR(60)*
		8.39	90.0 ~ 161.2	1.0	3	CL(64)
		8.51	27.6 ~ 166.6	1.0	22	CL(64)
		8.59	90.0 ~ 161.2	1.0	3	CL(64)
		8.79	90.0 ~ 161.2	1.0418	3	CL(64)
		8.82	18.6 ~ 170.6	1.0486	16	MC(64)
		8.99	90.0 ~ 161.2	1.0659	3	CL(64)
	A_{y0}	8.52	26.6 ~ 159.7	1.0	27	AL(93)
		8.52	49.3 ~ 150.6	1.0	10	AL(93)
		8.82	24.5 ~ 155.8	1.0	15	MO(69)
		8.83	59.1 ~ 132.7	1.0	5	MC(64)
	A_{0y}	8.52	49.3 ~ 150.6	1.0	10	AL(93)
		8.93	58.0 ~ 127.4	1.0	4	MC(70)
	A_{yy}	8.52	49.3 ~ 150.6	1.0	10	AL(93)
	A_{xz}	8.80	77.0 ~ 136.0	1.0	2	MC(69)
	R	8.82	43.6 ~ 76.9	1.2153	3	WE(78)
	A	8.82	43.6 ~ 76.9	0.8684	3	WE(78)
	D	8.82	43.6 ~ 76.9	1.0	3	WE(78)
9.5	$d\sigma/d\Omega$	9.19	90.0 ~ 161.2	0.9392	3	CL(64)
		9.39	90.0 ~ 161.2	1.0	3	CL(64)
		9.51	27.6 ~ 166.6	1.0	21	CL(64)
		9.59	90.0 ~ 161.2	1.0	3	CL(64)
		9.75	30.0 ~ 150.0	1.0295	25	LO(56)
		9.78	90.0 ~ 161.2	1.0397	3	CL(64)
		9.98	90.0 ~ 161.2	1.0707	3	CL(64)
	A_{y0}	10.01	26.7 ~ 159.7	1.0	27	AL(93)
		10.01	49.3 ~ 150.6	1.0	10	AL(93)
	A_{0y}	9.93	58.0 ~ 127.4	1.0	4	MC(70)
		10.01	49.3 ~ 150.6	1.0	10	AL(93)
	A_{yy}	10.01	49.3 ~ 150.6	1.0	10	AL(93)
19.48	$d\sigma/d\Omega$	19.48	16.0 ~ 172.0	1.0	25	HU(71)
	A_{y0}	19.40	50.0 ~ 132.8	1.0	13	BA(71)
	A_{0y}	19.40	50.0 ~ 130.6	1.0	11	BA(71)
		19.60	148.8	1.0	1	MU(78)
	A_{yy}	19.40	50.0 ~ 130.6	1.0	11	BA(71)
	A_{xx}	19.40	50.0 ~ 126.3	1.0	8	BA(71)
	σ_r	19.55	0.0	1.0	1	SO(76)

A best fit solution of PSA at each energy is obtained by varying the free parameters of $\delta_{\ell,J}, \rho_J^P$ and $\eta_{\ell,J}$ so as to minimize the χ^2 value:

$$\chi^2 = \sum_{ij} \left[\frac{\theta_{ij}^{\mathrm{th}} - n_j \theta_{ij}^{\mathrm{ex}}}{n_j \Delta_{ij}^{\mathrm{ex}}} \right]^2 + \sum_j \left[\frac{1 - n_j}{\Delta n_j} \right]^2 . \tag{4.42}$$

Here $\theta_{ij}^{\mathrm{ex}}$ is the experimental datum of observable i for the j-th experiment with the experimental error $\Delta_{ij}^{\mathrm{ex}}$, and $\theta_{ij}^{\mathrm{th}}$ is its theoretical value. Here n_j is the renormalization parameter assigned to the data of the j-th group.

4.2.4 Obtained solutions

The obtained solutions for single-energy PSA of p-^{3}He scattering at T_L = 4.0, 5.5, 6.8, 8.5, 9.5 and 19.48 MeV are shown in Table 4.2 with the χ^2-values and the total numbers of experimental data points N_t. The renormalization parameters n_j were used as free parameters for some data where the significant differences among the data groups exist. Hence a data group with $n_j \neq 1$ is different from data groups for the same observable with $n_j = 1$ in their θ_{cm}-dependence. We obtained good solutions at 4.0 and 5.5 MeV in both the MW and BB representations, together with the mixing parameters $\rho_J^P = \rho_1^{\pm}, \rho_2^{\pm}$ and ρ_3^-, where P is the parity in the total angular momentum J state. We give the phase-shift solutions at 4.0 MeV in both the MW and BB representations for comparison. Our obtained BB phase shifts at 4.0 MeV are consistent with those for the energy-dependent PSA of Alley and Knutson[113]. At 6.8, 8.5 and 9.5 MeV with the present database, it is not possible to complete single-energy PSA, so that the present PSA were carried out with the approximation $\rho_2^+ = \rho_2^- = \rho_3^- = 0$.

At 19.48 MeV, we performed the complete PSA with no approximations, and obtained a phase-shift solution in spite of the relatively small total number of data. This result seems to be due to the precise $d\sigma/d\Omega$ and A_{y0} data and the data for the three kinds of spin observables A_{0y}, A_{yy} and A_{xx}.

The widths of the error bars on the obtained parameters are given by the widths of the χ^2-valley at its minimum point, which were defined by Powell[38].

The observables calculated with the present PSA-solutions are given in Figs. 4.1 – 4.6 with the experimental data at each energy. At T_L = 19.48 MeV, the total reaction cross section predicted by our solution is σ_r = 48.02 mb for the experimental value given by Sourkes et al.[140], 44 $\pm$ 12 mb at T_L = 19.55 MeV.

4.2.5 Concluding remarks

We developed a computer program for the single-energy PSA of p-^{3}He scattering by using both the BB and MW representations. The program was applied to the analyses of data satisfying $T_L \leq$ 20 MeV. The obtained BB-phase shifts and their predicted observables for $T_L \lesssim$ 10 MeV were confirmed to be consistent with the solution of energy dependent PSA given by Alley and Knutson[113].

Table 4.2: Obtained phase-shift solutions.

Wave	T_L = 4.0 MeV		5.5	6.8
	χ^2/N_t = 143/136	145/136	77/151	101/120
	δ (MW)	δ (BB)	δ	δ
$^1S_0$	-53.1±2.4	-51.1±1.8	-65.9±1.0	-79.3±0.6
$^3S_1$	-50.2±0.8	-50.3±0.2	-58.5±0.4	-65.3±0.1
$^1P_1$	19.1±2.0	17.6±0.6	25.6±0.5	26.1±0.2
$^3P_0$	16.3±0.3	16.7±0.2	22.1±0.4	26.6±0.1
$^3P_1$	33.4±0.7	34.3±0.2	43.3±0.2	47.4±0.1
$^3P_2$	38.0±0.2	38.3±0.1	51.1±0.3	58.4±0.1
$^1D_2$	-0.894±0.653	-0.693±0.468	-0.407±0.585	-0.681±0.267
$^3D_1$	-0.865±0.438	-0.600±0.276	-1.55±0.29	-2.16±0.03
$^3D_2$	-1.74±0.39	-2.21±0.228	-2.01±0.25	-2.27±0.06
$^3D_3$	-0.830±0.166	-0.661±0.083	-1.44±0.29	-2.33±0.02
$^1F_3$	0.574±1.750	0.765±0.461	0.965±0.457	1.66±0.25
$^3F_2$	0.542±0.198	0.455±0.051	-0.0952±0.1010	0.475±0.025
$^3F_3$	-0.836±1.060	-0.823±0.149	0.176±0.152	-0.873±0.061
$^3F_4$	-0.0251±0.1540	-0.0796±0.0323	-0.0835±0.1840	0.333±0.019
ρ_1^+	-0.0043±0.0316	-0.905±0.804	-0.0363±0.0084	-0.0745±0.0114
ρ_1^-	-0.1327±0.1100	-13.5±0.3	-0.1808±0.1350	-0.206±0.099
ρ_2^+	-0.0026±0.1920	1.00±1.83	-0.0032±0.0394	
ρ_2^-	0.0381±0.0181	2.52±1.01	0.0285±0.0057	
ρ_3^-	-0.0009±0.0881	1.42±0.98	-0.0015±0.0544	
	8.5	9.5	19.48	
	χ^2/N_t = 137/145	88/122	46/70	
	δ	δ	δ	η
$^1S_0$	-87.8±0.4	-91.2± 0.3	-111.9±0.3	1.0
$^3S_1$	-69.8±0.1	-74.4± 0.1	-92.6±0.1	0.935 ± 0.004
$^1P_1$	23.1±0.1	26.3± 0.1	34.2±0.3	1.0
$^3P_0$	27.6±0.1	32.9±0.2	53.3±0.5	1.0
$^3P_1$	55.3±0.1	53.5±0.1	44.2±0.2	0.849 ±0.008
$^3P_2$	66.7±0.04	67.5±0.04	72.3±0.1	0.883±0.005
$^1D_2$	-2.42±0.17	-5.33±0.13	-0.206±0.260	1.0
$^3D_1$	-1.36±0.03	-1.98±0.03	3.76±0.45	0.888±0.008
$^3D_2$	-2.13±0.04	-1.78±0.05	-2.86±0.43	1.0
$^3D_3$	-1.99±0.02	-1.80±0.02	0.837±0.122	0.980±0.004
$^1F_3$	1.92±0.13	1.14± 0.11	0.189±0.166	1.0
$^3F_2$	1.04±0.02	1.28±0.02	3.78±0.16	1.0
$^3F_3$	-0.396±0.050	-0.0453±0.0519	3.67±0.16	1.0
$^3F_4$	1.11±0.02	1.21±0.02	4.85±0.09	1.0
ρ_1^+	-0.0682±0.0080	-0.0651±0.0073	-0.2719±0.0097	
ρ_1^-	-0.2587±0.0995	-0.265±0.1120	-0.4001±0.3490	
ρ_2^+			-0.0269±0.2510	
ρ_2^-			0.0827±0.0129	
ρ_3^-			-0.0166±0.1800	

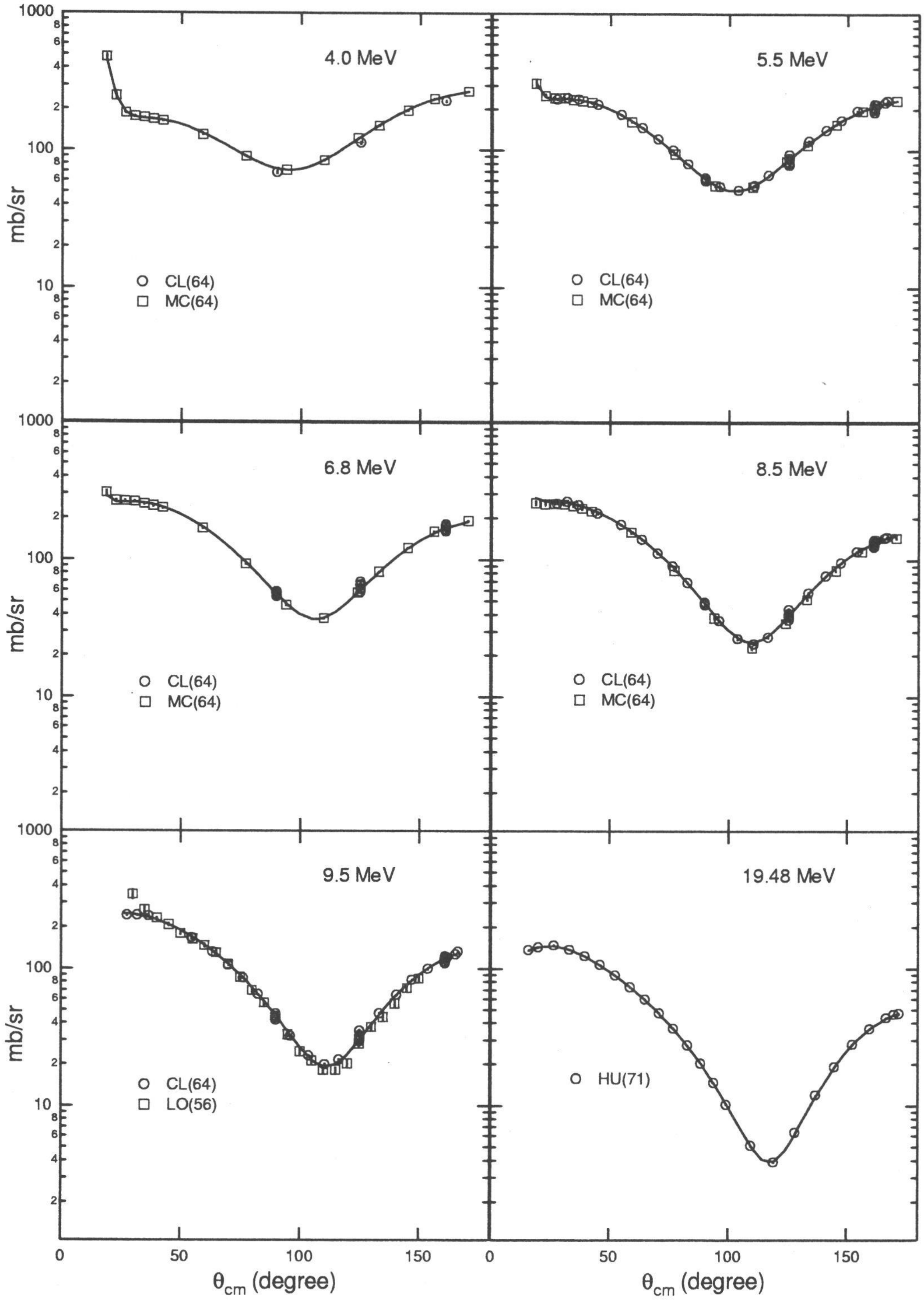

Figure 4.1: Prediction of the differential cross section (solid lines) by the solutions of PSA at T_L = 4.0, 5.5, 6.8, 8.5, 9.5 and 19.48 MeV, respectively. The correspondence of the experimental data in each graph is given in Table 4.1.

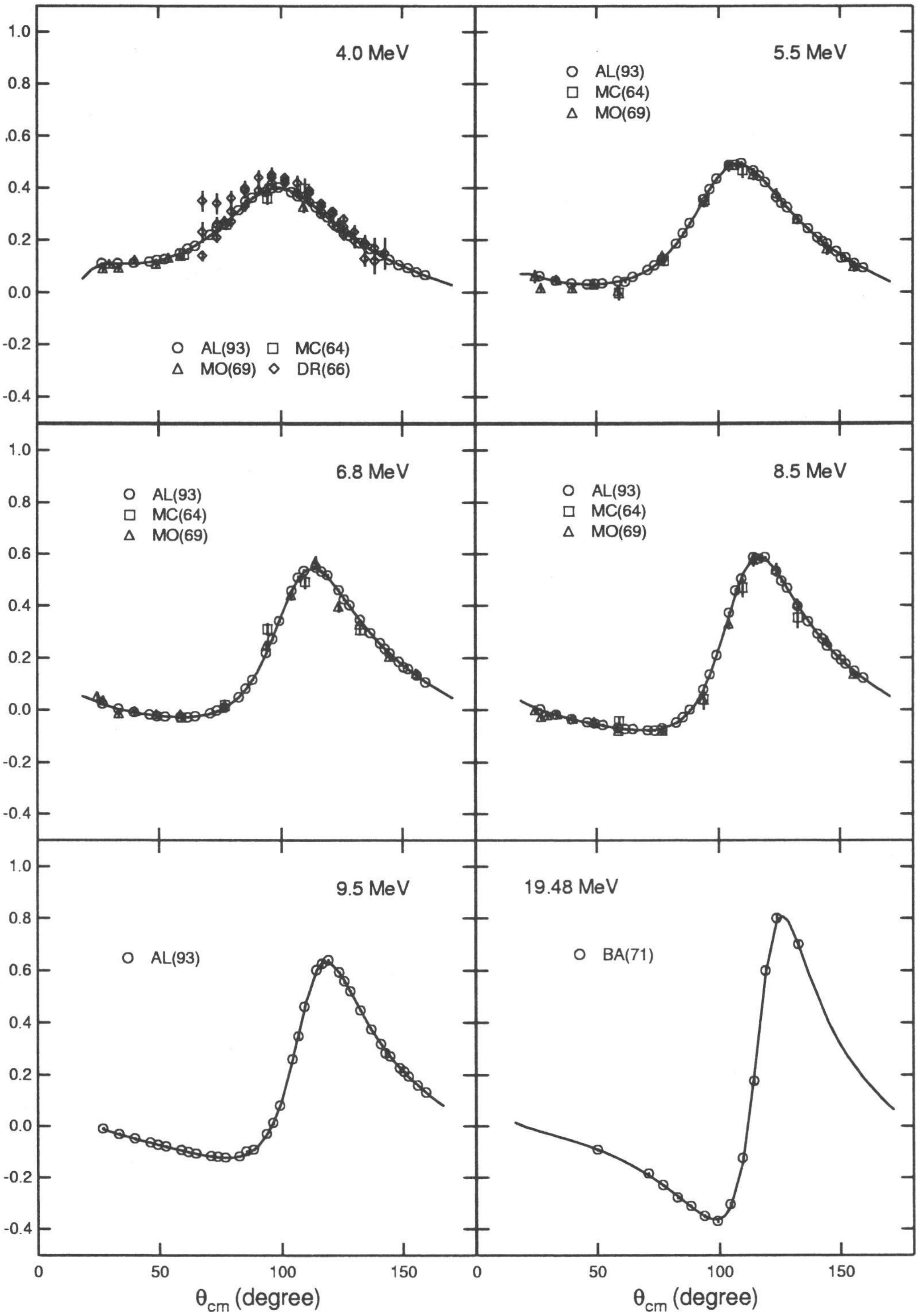

Figure 4.2: Prediction of the proton analyzing power (solid lines) by the solutions of PSA at T_L = 4.0, 5.5, 6.8, 8.5, 9.5 and 19.48 MeV, respectively. The correspondence of the experimental data in each graph is given in Table 4.1.

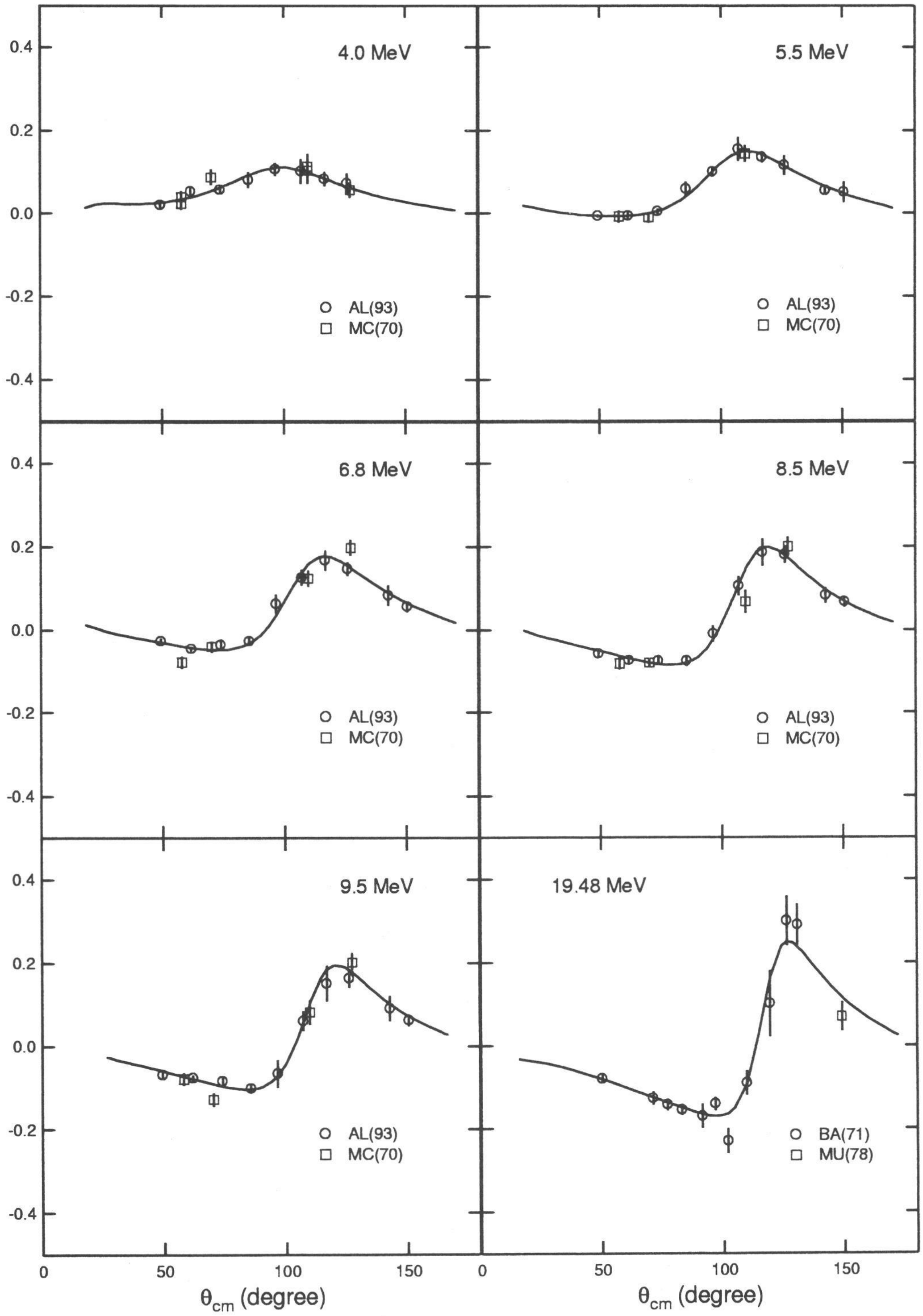

Figure 4.3: Prediction of the ^{3}He analyzing power (solid lines) by the solutions of PSA at T_L = 4.0, 5.5, 6.8, 8.5, 9.5 and 19.48 MeV, respectively. The correspondence of the experimental data in each graph is given in Table 4.1.

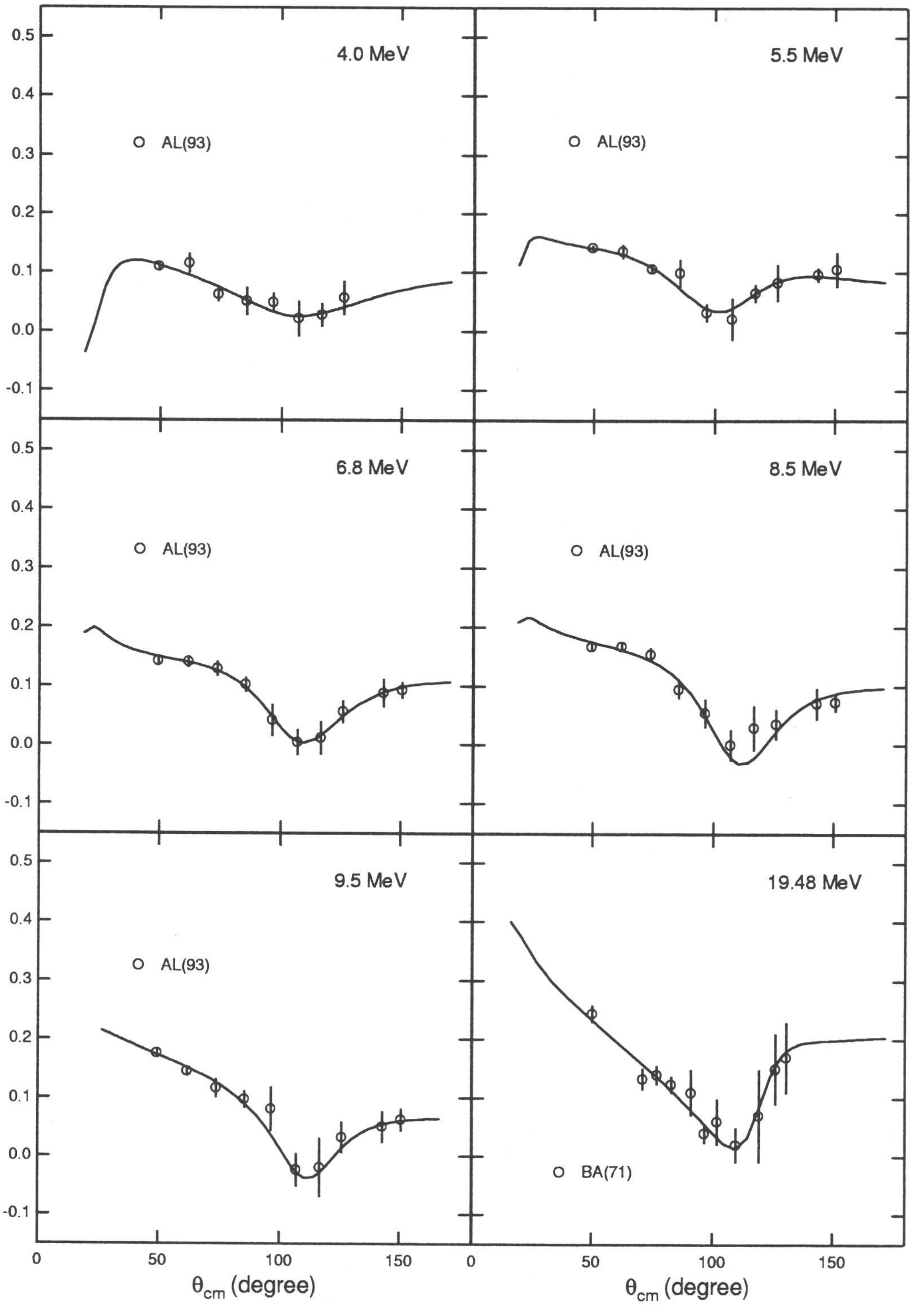

Figure 4.4: Prediction of the A_{yy} (solid lines) by the solutions of PSA at T_L = 4.0, 5.5, 6.8, 8.5, 9.5 and 19.48 MeV, respectively. The correspondence of the experimental data in each graph is given in Table 4.1.

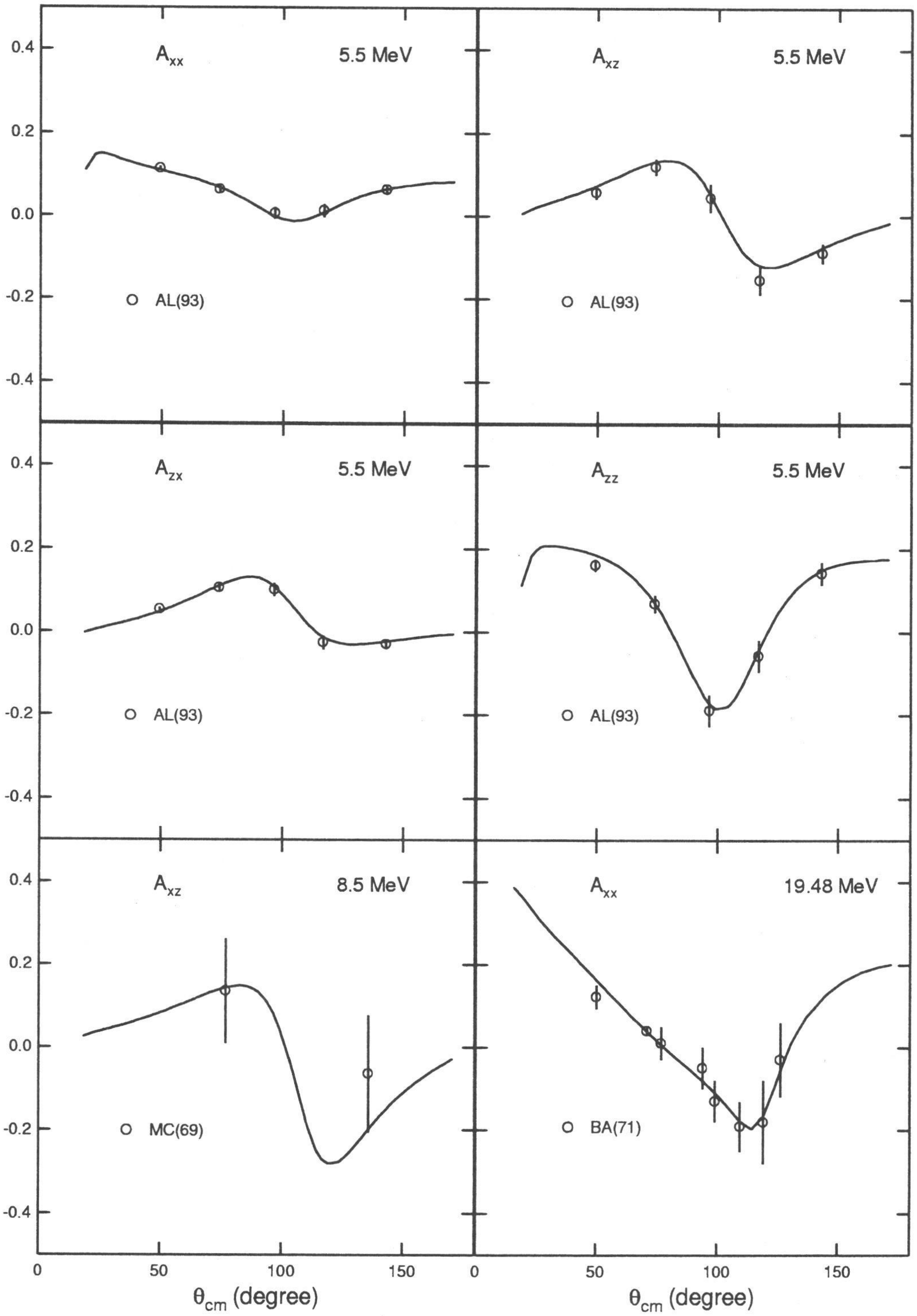

Figure 4.5: Prediction (solid lines) of A_{xx}, A_{xz}, A_{zx} and A_{zz} by PSA at 5.5 MeV, A_{xz} at 8.5 MeV and A_{xx} at 19.48 MeV, and their experimental data. The correspondence of the experimental data in each graph is given in Table 4.1.

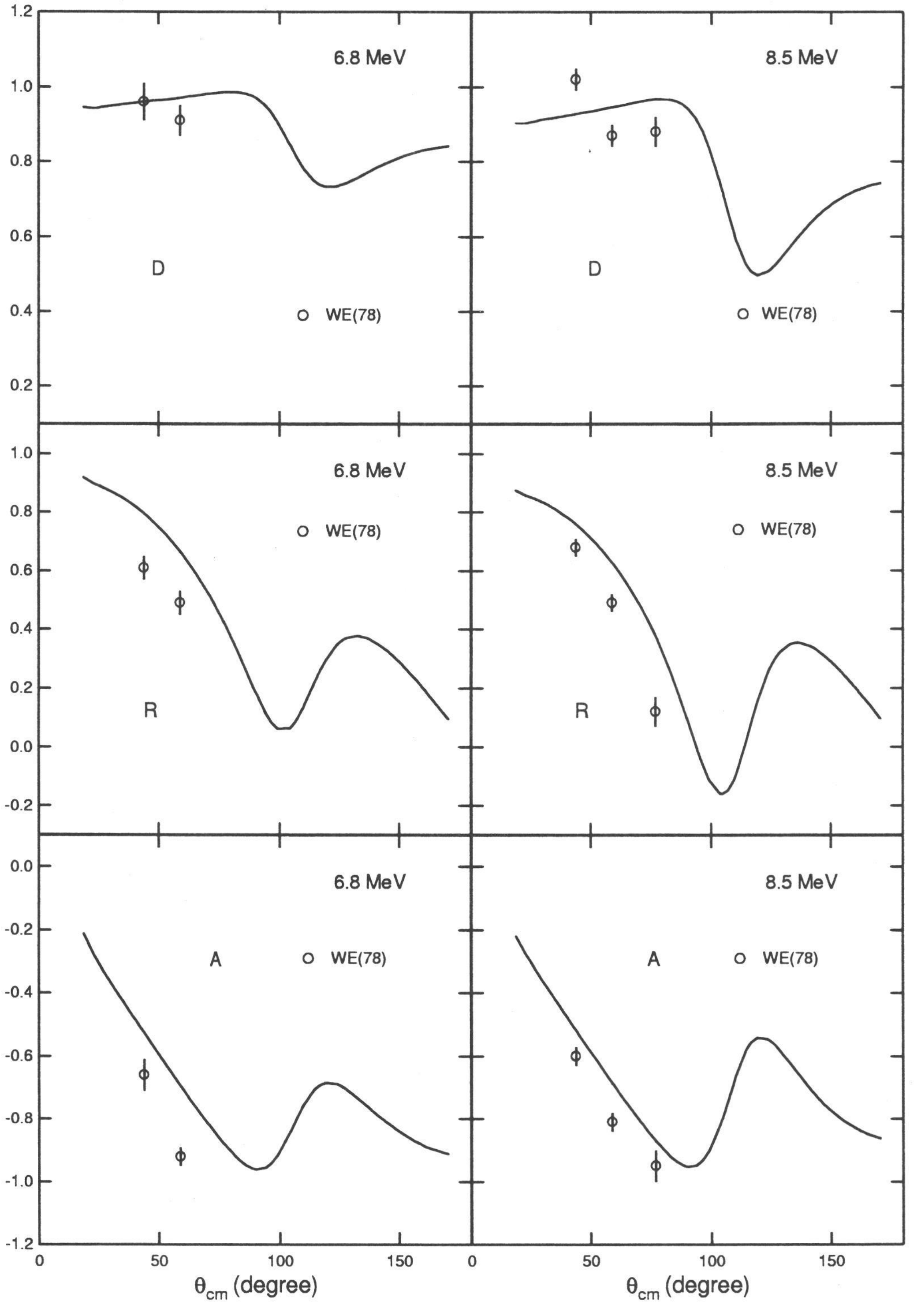

Figure 4.6: Prediction of the Wolfenstein parameters (solid lines) by the solutions of PSA at T_L = 6.8 and 8.5 MeV, respectively. The correspondence of the experimental data in each graph is given in Table 4.1.

In the analysis at $T_L = 19.48$ MeV, the inelastic effect was taken into account by fitting the datum of the total reaction cross section, and our program succeeded to determine the phase shifts and the reflection parameters.

Hereafter we wish to carry out the following studies:

(1) Determination of partial-wave amplitudes of p-^{3}He scattering for $T_L = 100 - 300$ MeV.

(2) Determination of n-^{3}He scattering amplitudes for $T_L \lesssim 300$ MeV.

(3) Search for the phenomenological p-^{3}He and n-^{3}He potentials from the nucleon-^{3}He scattering amplitudes determined by PSA.

The experimental data on n-^{3}He scattering are not sufficient to carry out project (2). Data on $d\sigma/d\Omega$, A_{y0} and A_{0y} for n-^{3}He scattering with $T_L \lesssim 300$ MeV are needed. In order to carry out the PSA for studies (1) and (2), we also need data on total reaction cross sections and on the other forward observables of p-^{3}He and n-^{3}He scatterings.

In the present analysis, it was found that the $^1P_1$-$^3P_1$ mixing effect in p-^{3}He scattering is significant, as is seen in Table 4.2. This effect is due to the anti-symmetric LS term $f(\boldsymbol{\sigma}_1 - \boldsymbol{\sigma}_2) \cdot \boldsymbol{n}$ in Eq. (4.30), which disappears in the nucleon-nucleon system. This means that the p-^{3}He potential should contain this term.